

# Determination of the $^{36}\text{Mg}(n, \gamma)^{37}\text{Mg}$ reaction rate from Coulomb dissociation of $^{37}\text{Mg}$

Shubhchintak<sup>1,\*</sup>, R. Chatterjee<sup>2,†</sup> and R. Shyam<sup>3‡</sup>

<sup>1</sup>*Department of Physics and Astronomy, Texas A&M University-Commerce, Commerce, Texas 75428, USA*

<sup>2</sup>*Department of Physics, Indian Institute of Technology, Roorkee 247667, India and*

<sup>3</sup>*Saha Institute of Nuclear Physics, 1/AF Bidhan Nagar, Kolkata 700064, India*

(Dated: June 27, 2021)

We use the Coulomb dissociation (CD) method to calculate the rate of the  $^{36}\text{Mg}(n, \gamma)^{37}\text{Mg}$  radiative capture reaction. The CD cross sections of the  $^{37}\text{Mg}$  nucleus on a  $^{208}\text{Pb}$  target at the beam energy of 244 MeV/nucleon, for which new experimental data have recently become available, were calculated within the framework of a finite range distorted wave Born approximation theory that is extended to include the projectile deformation effects. Invoking the principle of detailed balance, these cross sections are used to determine the excitation function and subsequently the rate of the  $^{36}\text{Mg}(n, \gamma)^{37}\text{Mg}$  reaction. We compare these rates to those of the  $^{36}\text{Mg}(\alpha, n)^{39}\text{Si}$  reaction calculated within a Hauser-Feshbach model. We find that for  $T_9$  as large as up to 1.0 (in units of  $10^9$  K) the  $^{36}\text{Mg}(n, \gamma)^{37}\text{Mg}$  reaction is much faster than the  $^{36}\text{Mg}(\alpha, n)^{39}\text{Si}$  one. The inclusion of the effects of  $^{37}\text{Mg}$  projectile deformation in the breakup calculations, enhances the  $(n, \gamma)$  reaction rate even further. Therefore, it is highly unlikely that the  $(n, \gamma)$   $\beta$ -decay  $r$ -process flow will be broken at the  $^{36}\text{Mg}$  isotope by the  $\alpha$ -process.

PACS numbers: 24.10.Eq, 25.60.Gc, 27.30.+t

## I. INTRODUCTION

It is generally believed that the  $r$ -process that synthesizes the heavy isotopes occurs under explosive conditions at high neutron densities and high temperatures [1–3]. The post-collapse phase of a type II or type Ib supernova can provide such a situation [4, 5]. In the early expanding phase, starting with a He-rich environment, the mass-8 gap would be bridged by either  $\alpha + \alpha + \alpha \rightarrow ^{12}\text{C}$  or  $\alpha + \alpha + n \rightarrow ^9\text{Be}$  reactions. The  $\alpha$ -capture reactions would continue until temperatures and densities become relatively low and the charged particle reactions almost cease. At this stage a very neutron-rich freeze-out takes place, which triggers further synthesis of the elements by the radiative neutron-capture process [6].

For calculations of the  $r$ -process nucleosynthesis the inclusion of neutron-rich light nuclei in the reaction network, has been shown to be important - they can change the heavy element abundances by as much as an order of magnitude [6, 7]. The  $r$ -process path involving neutron-rich nuclei can in principle, go up to the drip line isotope once equilibrium between  $(n, \gamma)$  and  $(\gamma, n)$  processes is established. If, however, the  $(\alpha, n)$  reaction becomes faster than the  $(n, \gamma)$  reaction on some “pre-drip line” neutron-rich isotope, then the  $r$ -process flow of the radiative neutron capture reaction followed by the  $\beta$ -decay is broken and the reaction path will skip the isotope on the drip line.

The abundance yields of extremely neutron rich nuclei show that the largest abundance is exhibited by the isotope of a given atomic number  $Z$  that is on or very close to the corresponding neutron-drip line. However,  $^{18}\text{C}$  and  $^{36}\text{Mg}$  are exceptions to this observation. Both these isotopes are still away from the respective drip lines of the corresponding  $Z$

values. For the carbon nucleus the drip line isotope is known to be  $^{22}\text{C}$  [8, 9], while for magnesium the drip line is extended upto  $^{40}\text{Mg}$  [10]. It was speculated in Ref. [6] that even at low temperatures (around  $T_9 = 0.62$ ), the rates of  $^{18}\text{C}(\alpha, n)^{21}\text{O}$  and  $^{36}\text{Mg}(\alpha, n)^{39}\text{Si}$  reactions can be larger than those of  $^{18}\text{C}(n, \gamma)^{19}\text{C}$  and  $^{36}\text{Mg}(n, \gamma)^{37}\text{Mg}$  reactions, respectively. To confirm this observation the precise determination of the rates of these reactions is of crucial importance.

The aim of this paper is to determine the rates of the  $^{36}\text{Mg}(n, \gamma)^{37}\text{Mg}$  reaction at the interaction kinetic energies that correspond to temperatures in the astrophysically interesting region ( $T_9 = 0.5 - 10$ ). Since,  $^{36}\text{Mg}$  has a very small half-life ( $\approx 5$  ms) [11], a direct measurement of the cross section of the reaction  $^{36}\text{Mg}(n, \gamma)^{37}\text{Mg}$  is not feasible at present. The situation is further complicated by the fact that temperatures  $T_9$  with values in the region of 0.5 - 10 correspond roughly to the center-of-mass (c.m.) energies in the range of 50 keV to 1.0 MeV. Thus rates of the  $^{36}\text{Mg}(n, \gamma)^{37}\text{Mg}$  reaction are of astrophysical importance for such low neutron kinetic energies, where performing measurements is prohibitively difficult.

However, with a beam of  $^{37}\text{Mg}$  it is possible to measure the cross section of the reverse reaction  $^{37}\text{Mg}(\gamma, n)^{36}\text{Mg}$  (photodisintegration process), and use the principle of detailed balance to deduce from it the cross sections of the  $^{36}\text{Mg}(n, \gamma)^{37}\text{Mg}$  reaction. A very promising way of studying the photodisintegration process is provided by the virtual photons acting on a fast charged nuclear projectile passing through the Coulomb field of a heavy target nucleus [12–14]. The advantage of this Coulomb dissociation (CD) method, in which the valence neutron is removed from a fast projectile in the Coulomb field of heavy target nuclei, is that here measurements can be performed at higher beam energies, which enhances the cross sections considerably. At higher energies the fragments in the final channel emerge with larger velocities that facilitates their more accurate detection. Furthermore, the choice of the adequate kinematical condition of the coincidence measurements allows the study of the low relative en-

\* Shubhchintak@tamuc.edu

† rcfphph@iitr.ac.in

‡ radhey.shyam@saha.ac.in

ergies of the final state fragments and ensures that the target nucleus remains in the ground state during the reaction (see, e.g., Refs. [15, 16]).

With the advent of new generation of radioactive ion beam facilities, it has become possible to produce a beam of  $^{37}\text{Mg}$  of sufficient quality to perform the measurements for the cross sections of the one-neutron removal reaction off this nucleus on a  $^{208}\text{Pb}$  target at a beam energy of 244 MeV/nucleon [17]. The corresponding data were analyzed within a post-form finite range distorted-wave Born approximation (FRDWBA) theory that is extended to include projectile deformation effects [18, 19]. From a comparison of calculations with the available experimental data it was concluded that the likely configuration of the  $^{37}\text{Mg}$  ground state is either  $^{36}\text{Mg}(0^+) \otimes 2p_{3/2}n$  or  $^{36}\text{Mg}(0^+) \otimes 2s_{1/2}n$  with the one neutron separation energy ( $S_n$ ) values of  $0.35 \pm 0.06$  MeV and  $0.50 \pm 0.07$  MeV, respectively. These values were found to be strongly dependent on the spectroscopic factors ( $C^2S$ ) and the deformation of the respective configuration.

In this work we use the Coulomb breakup cross section of  $^{37}\text{Mg}$  on a  $^{208}\text{Pb}$  target calculated within the FRDWBA theory as described above, to determine the photoabsorption cross sections  $^{37}\text{Mg}(\gamma, n)^{36}\text{Mg}$  by following the method of virtual photon number [12]. The later was then converted to  $(n, \gamma)$  capture cross section on  $^{36}\text{Mg}$  using the principle of detailed balance.

We adopt the cross sections of the  $^{36}\text{Mg}(\alpha, n)^{39}\text{Si}$  reaction as obtained from the Hauser-Feshbach (HF) code NON-SMOKER in Ref. [20].

In the next section we present our formalism, where the features of the FRDWBA theory as used in the calculations of the Coulomb dissociation cross sections are briefly described. We also outline the virtual photon number method for extracting the photo-dissociation cross sections from those of the Coulomb dissociation process. In Sec. III we present our results and discuss them. The summary and conclusions of our study are given in Sec. IV.

## II. FORMALISM

For non-degenerate stellar matter the rate ( $R$ ) of a nuclear reaction where two nuclei  $b$  and  $c$  ( $^{36}\text{Mg}$  and  $n$ , respectively, in our example) interact with relative energy  $E_{bc}$  to form a composite nucleus  $a$  ( $^{37}\text{Mg}$ ) via a radiative capture process (to be represented as  $[b(c, \gamma)a]$ , is given by (see, e.g., Refs. [7, 21]),

$$R = N_A \langle \sigma_{c\gamma}(v_{bc})v_{bc} \rangle, \quad (1)$$

where  $\sigma_{c\gamma}(v_{bc})$  is the cross section of the reaction between nuclei  $b$  and  $c$  with the relative velocity  $v_{bc}$  (which corresponds to relative energy  $E_{bc}$ ), and  $N_A$  is the Avogadro number ( $= 6.02 \times 10^{23}$  mole $^{-1}$ ). In Eq. (1) the product  $\sigma_{c\gamma}(v_{bc})v_{bc}$  is averaged over the Maxwell-Boltzmann velocity distribution.

$\langle \sigma_{c\gamma}(v_{bc})v_{bc} \rangle$  is written as

$$\langle \sigma_{c\gamma}(v_{bc})v_{bc} \rangle = \sqrt{\frac{8}{(k_B T)^3 \pi \mu_{bc}}} \int_0^\infty \sigma_{c\gamma}(E_{bc}) E_{bc} \times \exp\left(-\frac{E_{bc}}{k_B T}\right) dE_{bc}, \quad (2)$$

where  $\mu_{bc}$  is the reduced mass of the interacting nuclei,  $k_B$  is the Boltzmann constant, and  $T$  is the temperature of the stellar medium.

The prime nuclear physics input for calculating the rate of a particular radiative capture reaction is the cross section  $\sigma_{c\gamma}(E_{bc})$  at the relative energy  $E_{bc}$  - this energy is usually in the range of a few keV to a few MeV for most of the astrophysical sites. The direct measurement of this cross section in the laboratory is extremely difficult at these low energies. Even more serious is the fact that for most reactions of interest the target nuclei are radioactive, having very short half lives.

However, by invoking the principle of detailed balance, the capture cross section ( $\sigma_{c\gamma}$ ), can be calculated from the cross section  $\sigma_{\gamma c}$  of the time-reversed reaction  $a(\gamma, c)b$ , (photodisintegration cross section of  $a$ ) as,

$$\sigma_{c\gamma} = \frac{2(2j_a + 1)}{(2j_b + 1)(2j_c + 1)} \frac{k_\gamma^2}{k_{bc}^2} \sigma_{\gamma c}, \quad (3)$$

where  $j_a$ ,  $j_b$ , and  $j_c$  are the spins of particles  $a$ ,  $b$ , and  $c$ , respectively.  $k_\gamma$  is the photon wave number and  $k_{bc}$  is that of the relative motion between  $b$  and  $c$ .

Now, the two-body photodisintegration cross section can be related to the relative energy spectra of the three-body elastic Coulomb breakup reaction ( $a + t \rightarrow b + c + t$ ,  $t$  being a heavy target) as (see, e.g., Ref. [22])

$$\frac{d\sigma}{dE_{bc}} = \frac{1}{E_\gamma} \sum_\lambda n_{\Pi\lambda} \sigma_{\gamma c}, \quad (4)$$

where  $n_{\Pi\lambda}$  is the virtual photon number of type  $\Pi$  (electric or magnetic) and multipolarity  $\lambda$ . The photon energy is given by  $E_\gamma = E_{bc} + S_n$ , with  $S_n$  being the nucleon separation energy of the projectile  $a$ . The relative energy between the fragments  $b$  and  $c$  in the final channel is denoted by  $E_{bc}$ .

Combining Eqs. (3) and (4) we can express  $\sigma_{c\gamma}$  in terms of  $\frac{d\sigma}{dE_{bc}}$  as

$$\sigma_{c\gamma} = \frac{2(2j_a + 1)}{(2j_b + 1)(2j_c + 1)} 2\mu_{bc} \frac{E_\gamma^3}{E_{bc}} \frac{1}{n_{\Pi\lambda}} \frac{d\sigma}{dE_{bc}}, \quad (5)$$

where we assume that the Coulomb breakup cross section gets a contribution from a single multipolarity and type,  $\Pi\lambda$ .

For application to the calculations of the reaction of interest in the present work, we use a fully quantum mechanical theory of Coulomb breakup reactions to calculate the Coulomb dissociation of  $^{37}\text{Mg}$ , which is then used to extract the rate of the capture reaction  $^{36}\text{Mg}(n, \gamma)^{37}\text{Mg}$ . The theory of CD reactions used by us is formulated within the post-form (FRDWBA) [23], where the electromagnetic interaction between the fragments and the target nucleus is included to all orders

and the breakup contributions from the entire non-resonant continuum corresponding to all the multipoles and the relative orbital angular momenta between the fragments are taken into account. This theory was extended in Refs. [18, 19] so that it can also be used to calculate the CD of those nuclei that have deformed ground states. Full ground state wave function of the projectile, of any orbital angular momentum configuration, enters as an input into this theory, where we explicitly require only the ground state wave function of the projectile as an input.

Within the FRDWBA theory the cross sections for relative energy spectra for the elastic breakup reaction,  $a+t \rightarrow b+c+t$ , where projectile  $a$  (assumed to have a core  $b$  plus a valence particle  $c$  configuration) breaks up into fragments  $b$  and  $c$  in the Coulomb field of a target  $t$ , can be written as,

$$\frac{d\sigma}{dE_{bc}} = \int_{\Omega_{bc}, \Omega_{at}} d\Omega_{bc} d\Omega_{at} \left\{ \sum_{lm} \frac{1}{(2\ell+1)} |\beta_{\ell m}|^2 \right\} \times \frac{2\pi}{\hbar v_{at}} \frac{\mu_{bc} \mu_{at} p_{bc} p_{at}}{h^6}, \quad (6)$$

where  $v_{at}$  is the  $a-t$  relative velocity in the entrance channel,  $\Omega_{bc}$  and  $\Omega_{at}$  are solid angles,  $\mu_{bc}$  and  $\mu_{at}$  are reduced masses, and  $p_{bc}$  and  $p_{at}$  are appropriate linear momenta corresponding to the  $b-c$  and  $a-t$  systems, respectively.  $\ell$  and  $m$  are the relative orbital angular momentum and its projection, respectively. It may be noted that the projectile  $a$  can also be deformed.

If one of the fragments (say  $c$ ) is uncharged, the reduced transition amplitude,  $\beta_{\ell m}$ , for this reaction is given by [19]

$$\beta_{\ell m} = \left\langle e^{i(\gamma \mathbf{q}_c - \alpha \mathbf{K}) \cdot \mathbf{r}_1} |V_{bc}(\mathbf{r}_1)| \phi_a^{\ell m}(\mathbf{r}_1) \right\rangle \times \left\langle \chi_b^{(-)}(\mathbf{q}_b, \mathbf{r}_i) e^{i\delta \mathbf{q}_c \cdot \mathbf{r}_1} | \chi_a^{(+)}(\mathbf{q}_a, \mathbf{r}_i) \right\rangle. \quad (7)$$

The ground state wave function of the projectile  $\phi_a^{\ell m}(\mathbf{r}_1)$  appears in the first term (vertex function), while the second term that describes the dynamics of the reaction, contains the Coulomb distorted waves  $\chi^{(\pm)}$ . This can be expressed in terms of the bremsstrahlung integral.  $\alpha$ ,  $\gamma$ , and  $\delta$  are the mass factors pertaining to the three-body Jacobi coordinate system (see Fig. 1 of Ref. [19]). In Eq. (7),  $\mathbf{K}$  is an effective local momentum appropriate to the core-target relative system and  $\mathbf{q}_i$  ( $i = a, b, c$ ) are the Jacobi wave vectors of the respective particles.

$V_{bc}(\mathbf{r}_1)$  [in Eq. (7)] is the interaction between  $b$  and  $c$ , in the initial channel. We introduce an axially symmetric quadrupole-deformed potential, as

$$V_{bc}(\mathbf{r}_1) = V_0 f(r_1) - \beta_2 R V_0 \frac{df(r_1)}{dr_1} Y_2^0(\hat{\mathbf{r}}_1), \quad (8)$$

where  $V_0$  is the depth of the spherical Woods-Saxon potential and  $f(r_1) = [1 + \exp(\frac{r_1 - R}{a_0})]^{-1}$ , with  $R = r_0 A^{1/3}$ ,  $r_0$  and  $a_0$ , the radius and diffuseness parameters, respectively.  $\beta_2$  is the quadrupole deformation parameter. The first part of Eq. (8) is the spherical Woods-Saxon potential  $V_s(r_1)$ . Because of the deformation, the radial wave function of a given  $\ell$  corresponding to the full potential  $V_{bc}$ , has an admixture of wave

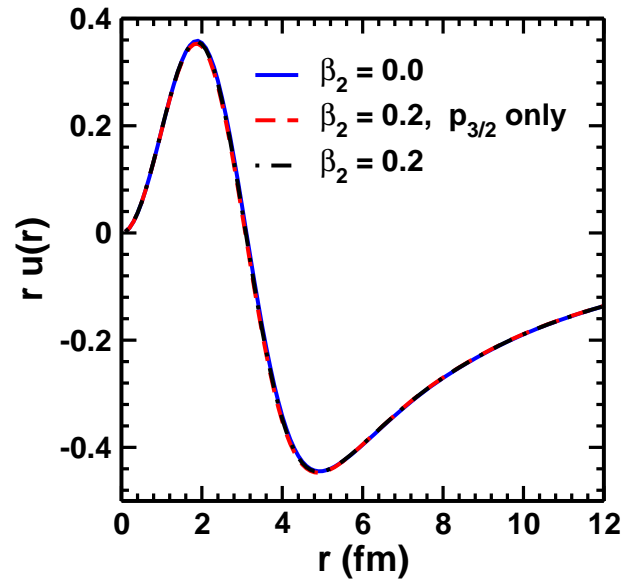


FIG. 1. Comparison of the wave functions calculated by solving the Schrödinger equation with potential given by Eq. (7). The  $S_n$  value is taken to be 0.35 MeV for the state  $2p_{3/2}$ . The wave function  $[ru(r)]$  obtained with the deformations parameter  $\beta_2 = 0.0$  (i.e., calculated with spherical potential) is shown by the solid line.  $ru(r)$  obtained with  $\beta_2 = 0.2$  but including only the component corresponding to  $\ell = 1$  and  $j = 3/2$  is shown by the dashed line while that including components with  $\ell = 1, 3, 5$  and all the allowed  $j$  values is displayed by the dashed-dotted line. All the wave functions are normalized to unity.

functions corresponding to the other  $\ell$  values of the same parity. However, we calculate the radial part of the ground state wave function of the projectile using the undeformed Woods-Saxon potential – this allows us to evaluate the structure part of the amplitude in Eq. (7) analytically. This approximation is justified because it has been shown in Ref. [24] that in a realistic deformed potential the relative motion wave function of the neutron is dominated by the lowest angular momentum component in the limit of small binding energy of the valence neutron, which is independent of the extent of the deformation.

To substantiate this point further, we show in Fig. 1 the wave function  $[ru(r)]$  obtained by solving the Schrödinger equation with the potential given by Eq. (8), taking the  $S_n$  value of 0.35 MeV. All the parameters of the potential were taken to be the same as those described above. We show results for  $\beta_2 = 0.0$  (solid line) and 0.2 (dashed and dashed-dotted lines). The dashed line corresponds to the case when for  $\beta_2 = 0.2$ , only  $\ell = 1$  and  $j = 3/2$  component was included, while the dashed-dotted line represents the wave function where for  $\beta_2 = 0.2$ , all the components corresponding to  $\ell = 1, 3$ , and 5 with all the allowed  $j$  values are included. All the three wave functions are normalized to 1 to make the comparison easier. We see that the solid and dashed curves are almost identical. The differences between the solid and dashed-dotted curves are also insignificant. This signifies that the deformation effects leave the wave functions calculated with the spherical

potentials unchanged. Furthermore, contributions of  $\ell > 1$  components to  $2p_{3/2}$  wave function are negligibly small.

Therefore, we perform our CD calculations with the spherical wave function corresponding to the orbital angular momentum of 1 ( $2p_{3/2}$  component), but taking Eq. (8) for the potential  $V_{bc}$ . One advantage of our this choice is that this allows us to calculate a substantial portion of our amplitude analytically. We emphasize that the deformation parameter ( $\beta_2$ ) still enters into the amplitude via  $V_{bc}$  in Eq. (7). For more details on the Coulomb dissociation formalism we refer to Ref. [19].

One can then relate the cross section in Eq. (6) to the photodissociation cross section,  $\sigma_{\gamma c}$ , for the reaction  $a(\gamma, c)b$ , by using Eq. (4). The virtual photon number appearing in this equation was calculated by following the same method as that used in Ref. [25].

Of course, the procedure of relating the CD cross section to that of the photodisintegration is valid only when transitions of a single multipolarity and type dominate the breakup cross section and the nuclear breakup effects are negligible. The validity of both these assumptions has been checked in several previous studies of the Coulomb dissociation reactions (see, eg., Refs. [13, 22, 26–29]). Nevertheless, in the context of the reaction studied in this paper, we checked that the breakup cross sections are indeed dominated by the  $E1$  multipolarity by evaluating the Coulomb dissociation cross sections within the first order Coulomb excitation theory [25]. Because the higher order effects that are included in the FRDWBA theory are negligible at higher beam energies as is shown in Ref. [30], this procedure should be sufficient to satisfy that the FRDWBA cross sections are indeed dominated by the  $E1$  multipolarity. Furthermore, at higher beam energies and forward angles (where the breakup data studied in Ref. [19] were taken), the nuclear breakup effects are negligible. Therefore, necessary conditions for the validity of Eq. (5) are fulfilled for the present case. We emphasize, however, that, in general, the validity of Eq. (5) must be checked in each case before using this to extract the photodissociation cross section.

Once the photodissociation cross sections are determined, one can extract the radiative capture cross sections by using Eq. (3) and use them in Eq. (2) to determine the rate of the reaction.

### III. RESULTS AND DISCUSSIONS

As discussed above, in the calculations of the CD cross sections within our theory, we require the single-particle wave function that describes the  $c - b$  relative motion in the ground state of the projectile for a given neutron-core configuration. This is obtained by solving the Schrödinger equation with a central Woods-Saxon type of potential with parameters  $r_0$  and  $a_0$  having values of 1.24 and 0.62 fm, respectively. The depth of this well is adjusted to reproduce the valence neutron separation energy corresponding to the adopted configuration. In Ref. [19], it was concluded that the ground state of  $^{37}\text{Mg}$  can have either of the configurations  $^{36}\text{Mg}(0^+) \otimes 2p_{3/2}n$  and  $^{36}\text{Mg}(0^+) \otimes 2s_{1/2}n$ , with  $S_n$  values of  $0.35 \pm 0.06$  MeV or  $0.50 \pm 0.07$  MeV, respectively and a  $C^2S$  of 1. However, for the

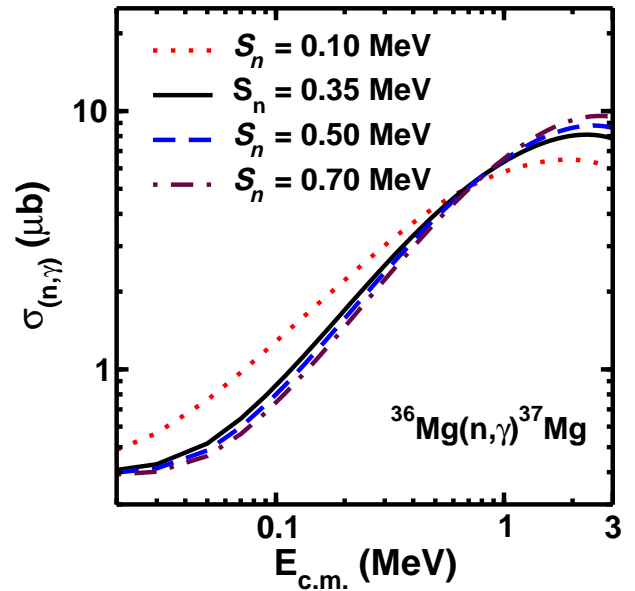


FIG. 2. Direct capture (DC) cross sections to the ground state (GS) of  $^{37}\text{Mg}$ , obtained by calculating the Coulomb dissociation of  $^{37}\text{Mg}$  on a  $^{208}\text{Pb}$  target at the beam energy of 244 MeV/nucleon for different values of one neutron separation energies ( $S_n$ ). Results for  $S_n$  values of 0.10, 0.35, 0.50 and 0.70 MeV, are shown by dotted, solid, dashed, and dashed-dotted lines, respectively. In these calculations the deformation parameter of the  $^{37}\text{Mg}$  ground state was taken to be 0 through out. The spectroscopic factor  $C^2S$  was unity in each case.

configuration  $^{36}\text{Mg}(0^+) \otimes 2p_{3/2}n$  the calculated one-neutron removal cross section overlaps with the corresponding experimental data band for the quadrupole deformation parameter ( $\beta_2$ ) below 0.32, which is in line with the predictions of the Nilsson model calculations of Ref. [31]. On the other hand, with the configuration  $^{36}\text{Mg}(0^+) \otimes 2s_{1/2}n$ , the calculations of Ref. [19] is unable to put any constraint on the parameter  $\beta_2$ . Therefore, we adopt the configuration  $^{36}\text{Mg}(0^+) \otimes 2p_{3/2}n$  with a  $S_n$  value of 0.35 MeV and a  $C^2S$  of 1 for the  $n-^{36}\text{Mg}$  relative motion in the ground state of  $^{37}\text{Mg}$ . The values of the searched depths of the Woods-Saxon well with shape parameters as given above, were found to be 44.42, 45.21, 45.94, and 46.60 MeV for  $S_n$  values of 0.10, 0.35, 0.50, and 0.70 MeV, respectively. It should, however, be mentioned here that the extracted value of  $S_n$  is sensitively dependent on  $C^2S$  as well as on the deformation parameter  $\beta_2$  of the  $^{37}\text{Mg}$  ground state. Since, definite knowledge about the later two quantities are still lacking we have chosen to show results for a range of  $S_n$  and  $\beta_2$  values.

We calculated the capture cross sections ( $\sigma_{n,\gamma}$ ) of the  $^{36}\text{Mg}(n, \gamma)^{37}\text{Mg}$  reaction as a function of the c.m. relative energy ( $E_{bc} = E_{\text{c.m.}}$ ) between the neutron and  $^{36}\text{Mg}$  ground state [ $^{36}\text{Mg}(0^+)$ ] for several values of  $S_n$  and  $\beta_2$ , using the Coulomb breakup cross section obtained in our FRDWBA model. In Fig. 2, we show  $\sigma_{n,\gamma}$  as a function of  $E_{\text{c.m.}}$  (in the range of 0 – 3 MeV) for  $S_n$  values of 0.10, 0.35, 0.50, and 0.70 MeV corresponding to a fixed  $\beta_2$  parameter of 0.0. We note in this figure that while for  $E_{\text{c.m.}}$  below 1 MeV,  $\sigma_{n,\gamma}$  are larger for

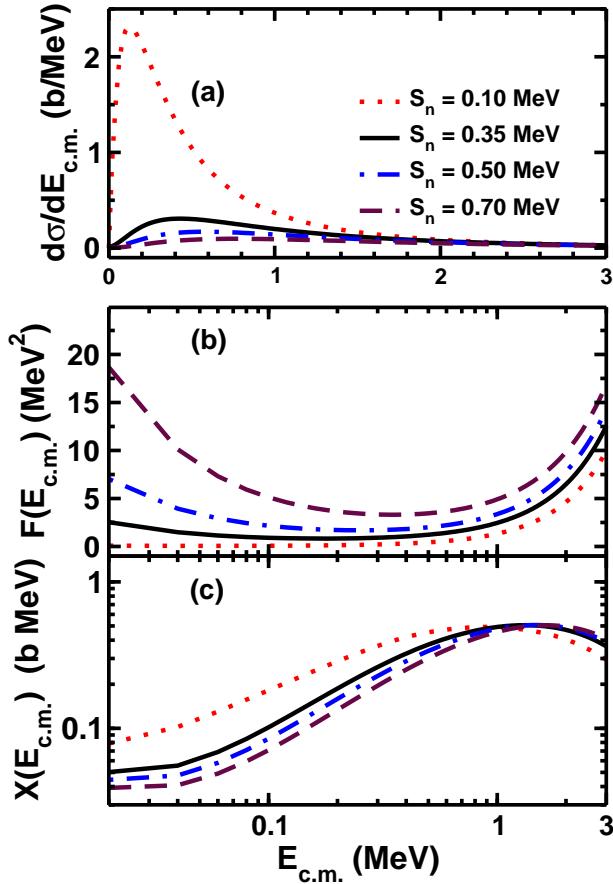


FIG. 3. (a) The Coulomb dissociation cross section  $d\sigma/dE_{c.m.}$  calculated for different values of  $S_n$  as a function of  $E_{c.m.}$ . (b) The kinematical factor  $F(E_{c.m.}) = [(E_{c.m.} + S_n)^3/E_{c.m.}]$  as a function of  $E_{c.m.}$  for various values of  $S_n$ . (c) The product of  $F(E_{c.m.})$  and  $d\sigma/dE_{c.m.}$  as a function of  $E_{c.m.}$  for various values of  $S_n$ .

smaller values of  $S_n$ , this trend is reversed for  $E_{c.m.}$  larger than 1 MeV, where the cross sections increase with increasing  $S_n$ . The reason for this observation is discussed below.

To understand the behavior of the  $\sigma_{n,\gamma}$  as a function of  $E_{c.m.}$  and  $S_n$  as seen in Fig. 2, we note from Eq. (5) that the capture cross sections obtained from the Coulomb dissociation method involves together with the CD cross section, the kinematical factor  $F(E_{c.m.}) = [(E_{c.m.} + S_n)^3/E_{c.m.}]$  and the inverse of the virtual photon number  $n_{\text{PL}}$ . In Fig. 3, we show the CD cross section [Fig. 3(a)], the kinematical factor  $F(E_{c.m.})$  [Fig. 3(b)], and their product,  $X(E_{c.m.})$  [Fig. 3(c)], as a function of  $E_{c.m.}$  for various values of  $S_n$ .

The Coulomb dissociation cross section shows the characteristics typical of the drip line nuclei having small one-neutron separation energies, where the breakup cross section is dominated by the low-lying dipole  $B(E1)$  strength (see, e.g., Ref. [32]), which leads to these cross sections peaking strongly near the smaller binding energies. This implies that a low-lying bound state leads to a peak in the low lying continuum, and the width and location of that peak is directly related to the location of the bound state pole. As the binding energy changes, the strength distribution changes in both the shape

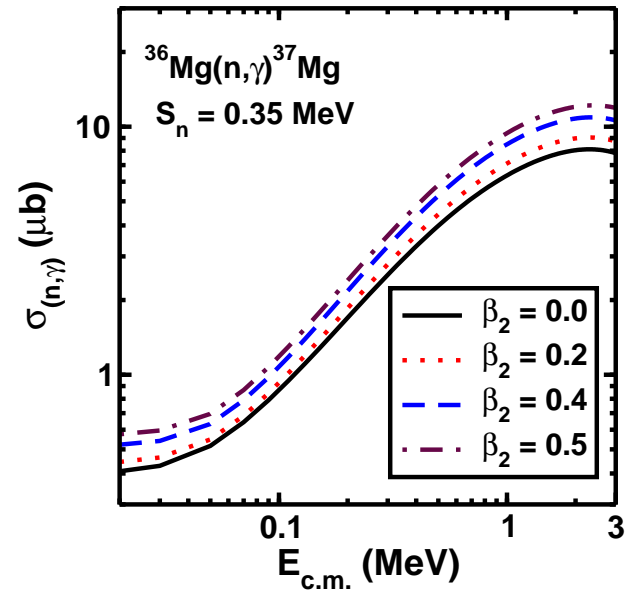


FIG. 4. Same as in Fig. 2 obtained by using CD cross sections calculated with different  $\beta_2$  values for a fixed  $S_n$  of 0.35 MeV. Results for  $\beta_2$  values of 0.0, 0.2, 0.4, and 0.5, are shown by solid, dotted, dashed, and dashed-dotted lines, respectively.

and the absolute value, which is apparent from Fig. 3(a).

In Fig. 3(b), we have shown the kinematical factor  $F(E_{c.m.})$  as a function of  $E_{c.m.}$  for various values of  $S_n$ . We note that  $F(E_{c.m.})$  is smallest in magnitude for the lowest value of  $S_n$  and it increases gradually with  $E_{c.m.}$  after some very small values of  $E_{c.m.}$ . As a result the product of  $F(E_{c.m.})$  and the CD cross sections [ $X(E_{c.m.})$ ], is still larger for smaller  $S_n$  but only for  $E_{c.m.} < 1$  MeV. However, for  $E_{c.m.}$  larger than this value, this behavior is reversed - now  $X(E_{c.m.})$  corresponding to the larger  $S_n$  becomes larger. This is understandable because the CD cross section remains approximately constant for  $E_{c.m.} > 1$  MeV, while  $F(E_{c.m.})$  is bigger for larger values of  $S_n$ . Furthermore, the virtual photon numbers have larger magnitudes for smaller  $S_n$  for  $E_{c.m.} < 1$  MeV, but they are of almost of similar values for all  $S_n$  for  $E_{c.m.} > 1$  MeV. This combined with  $X(E_{c.m.})$  leads to the behavior of the capture cross sections shown in Fig. 2, which appears to have a different  $S_n$  dependence as compared to that of the Coulomb dissociation cross sections particularly for  $E_{c.m.} > 1$  MeV. However, the capture cross sections corresponding to lower  $S_n$  is larger at  $E_{c.m.}$  below 1 MeV.

In Fig. 4, we show  $\sigma_{n,\gamma}$  as a function of  $E_{c.m.}$  for the deformation parameter values of  $\beta_2$  of 0.0, 0.2, 0.4, and 0.5, corresponding to a fixed  $S_n$  of 0.35 MeV and the spectroscopic factor of 1. In this case sensitivity of the cross section to the deformation parameter is seen also for  $E_{c.m.}$  below 1.0 MeV. We see that  $\sigma_{n,\gamma}$  increases with increasing  $\beta_2$ , which reflects the trend seen in the  $\beta_2$  dependence of the CD cross sections.

In our calculations the  $\beta_2$  dependence of the CD cross sections and hence that of the capture cross section results primarily from the fact that this parameter enters into the reaction amplitude explicitly through the potential  $V_{bc}$  [see Eq. (7)].

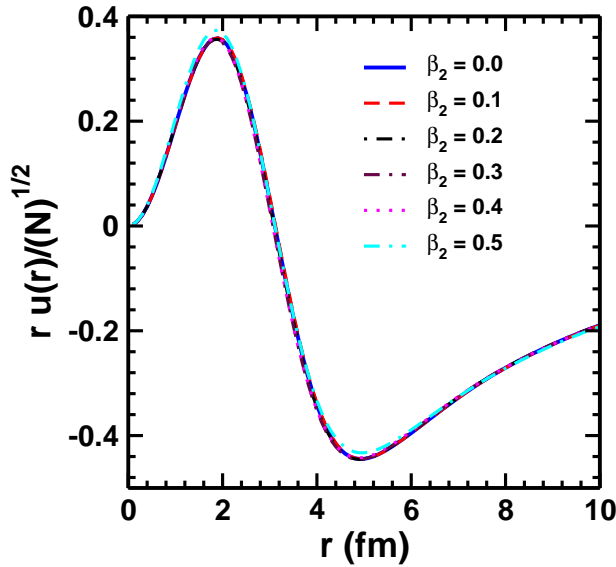


FIG. 5. Total wave function  $[ru(r)]$  for the  $\ell = 1$  and  $j = 3/2$  state including components with  $\ell = 1, 3, 5$  and all the allowed  $j$  values for different  $\beta_2$  parameters. All the wave functions are normalized to unity.

Had this not been the case, there would be no dependence of the cross sections on the  $\beta_2$  as these peripheral reactions are governed mainly by the asymptotic normalization coefficient (ANC), which is independent of the  $\beta_2$ , as is shown in Table I for the  $p_{3/2}$  state wave function.

TABLE I. Asymptotic normalization constant (ANC) for the deformed  $^{37}\text{Mg}$  wave function for different values of the deformation parameter  $\beta_2$ . The deformed wave functions are obtained by solving the Schrödinger equation with potential given by Eq. (7) with a  $S_n$  value of 0.35 MeV. Results are shown only for  $\ell = 1$  and  $j = 3/2$  state for each value of the deformation parameter.

$\beta_2$	$\ell$	$j$	ANC ( $\text{fm}^{-1/2}$ )
0.0	1	3/2	0.383
0.1	1	3/2	0.383
0.2	1	3/2	0.380
0.3	1	3/2	0.377
0.4	1	3/2	0.374
0.5	1	3/2	0.370

Moreover, even the asymptotic part of the total wave function (which has contributions from components corresponding to  $\ell = 1, 3$ , and 5 with all the allowed  $j$  values), is unaffected by changes in  $\beta_2$ . This is illustrated in Fig. 5 where we plot the total wave function corresponding to different values of  $\beta_2$ . The wave function in each case is normalized to 1 to make the comparison easier and more meaningful. We see that the varying of  $\beta_2$  leaves the asymptotic part of the wave function completely unchanged, which is in agreement with the results

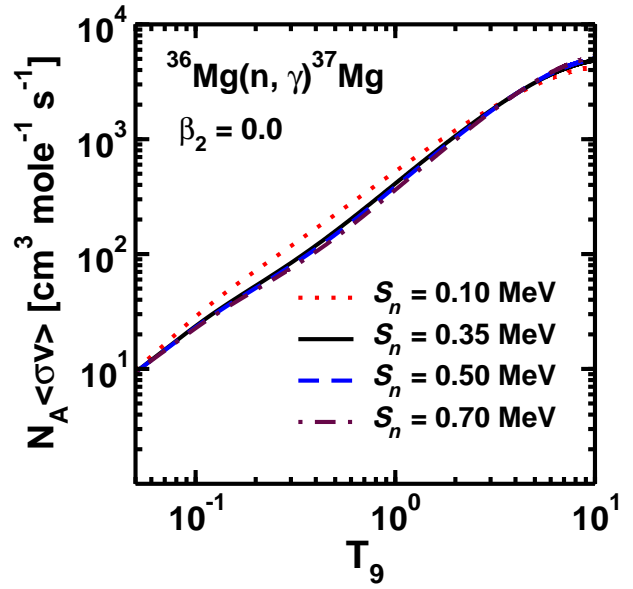


FIG. 6. Capture rates for the  $^{36}\text{Mg}(n, \gamma)^{37}\text{Mg}$  reaction as a function of temperature in units of  $10^9\text{K}$  ( $T_9$ ) for different values of  $S_n$  for a fixed  $\beta_2$  of 0.0.

shown in Ref. [33]. This further strengthens the fact that the  $\beta_2$  dependence of the CD cross section (and thus that of the capture cross section) is mainly due to the explicit presence of this parameter into the reaction amplitude.

The results for the capture cross sections shown in Figs. 2 and 4 correspond to the CD cross sections obtained with the configuration of  $^{36}\text{Mg}(0^+) \otimes 2p_{3/2}n$  for a  $C^2S$  value of 1. However, in Ref. [17] a  $C^2S$  of  $0.42 \pm 0.12$  was deduced for this configuration from an analyses of the data on Coulomb breakup within a semiclassical theory of this reaction. Even though this result is quite dependent on the theory of CD used in their analysis, had we used their value of  $C^2S$  our results would have been proportionately lower.

Reaction rates ( $R$ ) calculated from the capture cross sections are plotted in Figs. 6 and 7 as a function of  $T_9$  (the temperature equivalent of relative energy in units of  $10^9\text{K}$ , calculated from the relation  $E_{\text{c.m.}} = k_B T$ ). We recall that the experimental cross sections for the Coulomb breakup reaction  $^{37}\text{Mg} + \text{Pb} \rightarrow ^{36}\text{Mg} + n + \text{Pb}$ , involve uncertainties of about 15-20% [17], which should also be there in the calculated Coulomb dissociation cross sections that are fitted to these data. Therefore, the  $(n, \gamma)$  capture cross sections, and hence the rates of these reactions shown in Figs. 6 and 7, should also involve uncertainties of this order.

In Fig. 6 the reaction rate is shown for different values of  $S_n$  for a fixed  $\beta_2$  of 0.0, while in Fig. 7 it is shown for various values of  $\beta_2$  for a fixed  $S_n$  of 0.35 MeV. The ground state configuration of  $^{37}\text{Mg}$  remains the same as that in Figs. 2 and 4. We note that the reaction rate changes from  $10 \text{ cm}^3 \text{ mole}^{-1} \text{ s}^{-1}$  to about  $5000 \text{ cm}^3 \text{ mole}^{-1} \text{ s}^{-1}$  as  $T_9$  goes from 0.05 to 10. Its value around  $T_9 = 0.6$  is approximately  $200 \text{ cm}^3 \text{ mole}^{-1} \text{ s}^{-1}$ . The  $S_n$  and  $\beta_2$  dependencies of the reaction rate reflect the trends seen in the dependencies of the capture cross section on

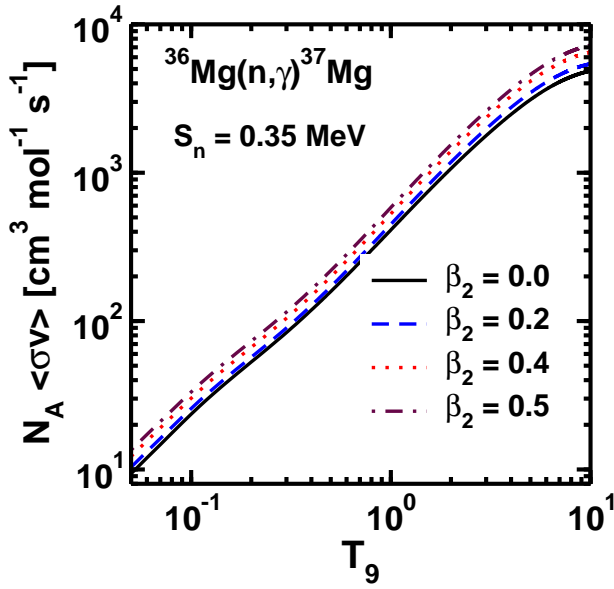


FIG. 7. Same as in Fig. 4 for different values of  $\beta_2$  for a fixed  $S_n$  of 0.35 MeV

these quantities, in Figs. 2 and 4. It may be noted that  $T_9$  in the range of 0.05 - 10 corresponds to  $E_{c.m.}$  approximately in the range 4 keV to 1 MeV.

As is evident from the integrand in Eq. (1), for a fixed stellar temperature, the maximum contribution to the reaction rate is strongly dependent on the reaction cross section and in turn on the relative energy. This is substantiated in Fig. 8, where we show the integrand of Eq. (1) as a function of  $E_{c.m.}$  for the reaction  $^{36}\text{Mg}(n, \gamma)^{37}\text{Mg}$  at different values of  $S_n$ , but fixed  $\beta_2$  and  $T_9$  of 0.0 and 1, respectively. We see that maximum contribution to the rate of this reaction comes from  $E_{c.m.}$  lying roughly between 0.2 - 0.3 MeV. At this low energy it is extremely difficult to measure reaction cross sections by direct methods. This is where the power of the CD method becomes evident as an indirect method in nuclear astrophysics. With the recent advances in experimental techniques it is possible to measure relative energy spectra at quite low relative energies in the CD experiments.

In Fig. 9, we show a comparison of the rates of  $^{36}\text{Mg}(n, \gamma)^{37}\text{Mg}$  and  $^{36}\text{Mg}(\alpha, n)^{39}\text{Si}$  reactions for the astrophysically relevant stellar temperature,  $T_9$ , in the range of 0.05 - 10. In calculations of the  $(n, \gamma)$  reaction the value of  $S_n$  is taken to be 0.35 MeV. Results are shown for  $\beta_2$  of 0.0 and 0.5. The rates of the  $(\alpha, n)$  reaction are calculated from the corresponding cross section given in Ref. [20] obtained from the NON-SMOKER code. We note that for  $T_9 \geq 2$  the  $^{36}\text{Mg}(\alpha, n)^{39}\text{Si}$  reaction is faster. Therefore, for these temperatures  $\alpha$  capture reactions are more efficient and the formation of elements of higher charge number ( $Z$ ) via the  $\alpha$ -induced processes is most important. However, at temperatures  $T_9$  below 2, the  $(\alpha, n)$  reaction becomes progressively slower and the  $(n, \gamma)$  reaction starts becoming more and more important. At these temperatures the classical  $r$ -process flow involving  $(n, \gamma)$  and  $(\gamma, n)$  reactions followed by  $\beta$  decay is much more

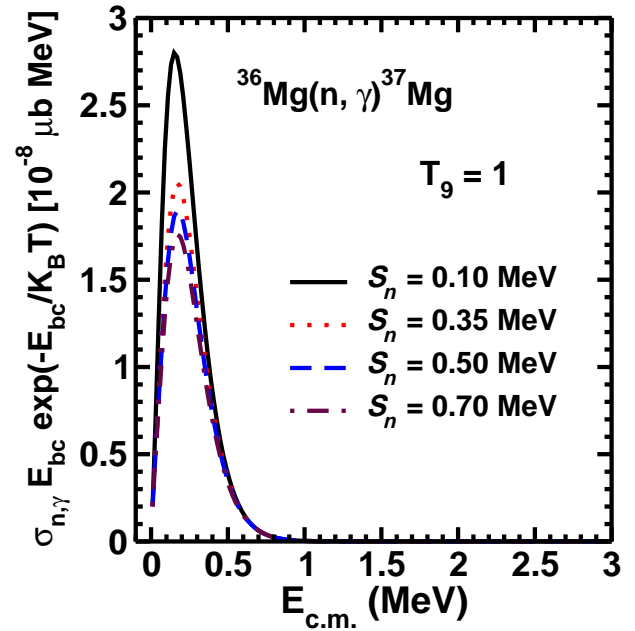


FIG. 8. Integrand of the reaction rate expression Eq. (1) as a function of  $E_{c.m.}$  for the  $^{36}\text{Mg}(n, \gamma)^{37}\text{Mg}$  reaction at different values of  $S_n$  for a fixed  $\beta_2$  of 0.0.

probable. In Fig. 9, we also note that the effect of projectile deformation is to increase the  $(n, \gamma)$  rates slightly over the no deformation case, but this is insignificant as far as main conclusion of this figure is concerned.

Also shown in Fig. 9 are the rates of the  $^{36}\text{Mg}(n, \gamma)^{37}\text{Mg}$  reaction obtained from the HF cross section reported in Ref. [20]. We notice that CD  $(n, \gamma)$  rates are significantly larger than those of the HF model. For  $T_9 \leq 1$  the difference between CD and HF rates is quite drastic (several orders of magnitude). However, the difference between them becomes relatively lesser and lesser as  $T_9$  increases beyond 1. The similar observation was also made in Ref. [7] for the case of the  $^{18}\text{C}(n, \gamma)^{19}\text{C}$  reaction. This emphasizes the need for accurate determination of the rates of the  $(n, \gamma)$  reaction on neutron rich light nuclei where the CD method can play a crucial role.

It is clear from Fig. 9 that around the equilibrium temperature,  $T_9 = 0.62$  where the main path of the reaction network runs through very neutron-rich nuclei, the  $^{36}\text{Mg}(n, \gamma)^{37}\text{Mg}$  reaction is much faster than the  $^{36}\text{Mg}(\alpha, n)^{39}\text{Si}$  reaction. Therefore, the  $(n, \gamma)$   $\beta$ -decay  $r$ -process is highly unlikely to be broken at the  $^{36}\text{Mg}$  isotope by the  $\alpha$ -process.

It is important to note that while HF cross sections have contributions only from the compound nuclear formations and decay mechanisms, the CD method produces only the direct capture component. In principle, both components coexist and need to be considered simultaneously when they are of the same order of magnitude.

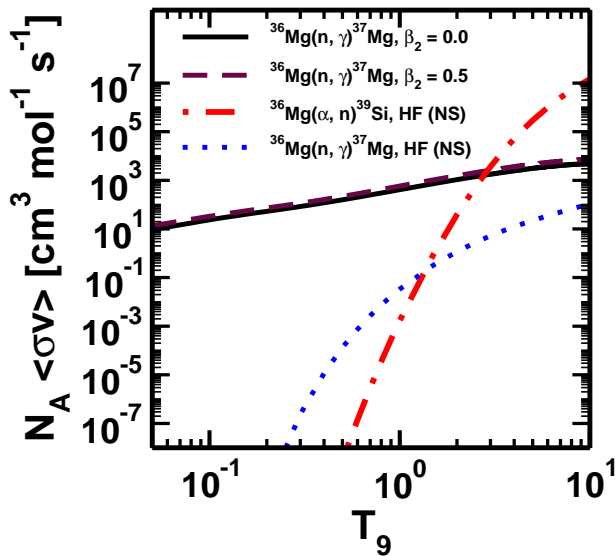


FIG. 9. Comparison of the rates of  $^{36}\text{Mg}(n, \gamma)^{37}\text{Mg}$  reaction calculated by the CD method using  $\beta_2$  parameters of 0 (solid line) and 0.5 (dashed line) (the neutron separation energy  $S_n$  was 0.35 MeV in both cases), with those of the  $^{36}\text{Mg}(\alpha, n)^{39}\text{Si}$  (dashed-dotted line) and  $^{36}\text{Mg}(n, \gamma)^{37}\text{Mg}$  (dotted line) reactions obtained from the Hauser Feshbach (HF) cross sections adopted from the Ref. [20] where they were obtained from the code NON-SMOKER(NS). The x-axis represents the temperature  $T_9$ .

#### IV. SUMMARY AND CONCLUSIONS

In summary, we calculate the rate of the  $^{36}\text{Mg}(n, \gamma)^{37}\text{Mg}$  reaction by studying the inverse photodissociation reaction in terms of the Coulomb dissociation of  $^{37}\text{Mg}$  on a  $^{208}\text{Pb}$  target at the beam energy of 244 MeV/nucleon using a theory formulated within the post-form finite range distorted-wave Born approximation that is extended to include the effects of the projectile deformation. This capture reaction is important in deciding if the  $r$ -process reaction flow will be sustained to Mg isotopes heavier than  $^{36}\text{Mg}$ . If the rate of this reaction is smaller than that of the  $^{36}\text{Mg}(\alpha, n)^{39}\text{Si}$  process, then the reaction flow will be broken at this point, thereby reducing the production of Mg isotopes with mass numbers larger than 36.

The advantage of our theoretical method is that it is free from the uncertainties associated with the multipole strength distributions of the projectile. In this approach measurements performed at beam energies in the range of few tens of MeV to few hundreds of MeV are used to extract cross sections of reactions at astrophysically relevant energies that usually lie in the range of few tens of keV to few hundreds of keV. Measurements performed at higher beam energies enhance the cross

sections considerably. At higher energies the fragments in the final channel emerge with larger velocities, which facilitates their more accurate detection. By choosing adequate kinematical conditions of the coincidence measurements, it becomes possible to study the final state fragments at low relative energies, and to ensure that the target nucleus remains in the ground state during the reaction.

Our calculations suggest that the consideration of the deformation of the projectile nucleus in the Coulomb dissociation calculations, does not have any significant effect on the rate of the  $^{36}\text{Mg}(n, \gamma)^{37}\text{Mg}$  reaction. Furthermore, the uncertainty in the value of one-neutron separation energy of the  $^{37}\text{Mg}$  nucleus also does not make any noticeable impact on the this rate.

We find that for stellar temperatures  $T_9$  above 2 the rates of the  $^{36}\text{Mg}(\alpha, n)^{39}\text{Si}$  reaction are larger than those of the  $^{36}\text{Mg}(n, \gamma)^{37}\text{Mg}$  reaction. This implies that at these temperatures the  $\alpha$ -capture reactions are more efficient than the neutron capture. Thus,  $\alpha$ -process operates at temperatures  $T_9 \geq 2$ . For lower temperatures ( $T_9$  below 2) however, the  $(\alpha, n)$  reaction rates become progressively smaller than those of the  $(n, \gamma)$  reaction. Eventually, the neutron capture becomes predominant and the classical  $r$ -process like flow, [ $(n, \gamma)$  and  $(\gamma, n)$  reactions followed by the  $\beta$  decay], becomes the key process.

It may be remarked that the Hauser-Feshbach model, which is adopted by us to get the rates of the  $^{36}\text{Mg}(\alpha, n)^{39}\text{Si}$  reaction, may not be a good approximation for the neutron rich nuclei. Nevertheless, we use these estimates because they are easy to obtain and their uncertainties are not larger than the differences seen between and  $(n, \gamma)$  and  $(\alpha, n)$  reaction rates in Fig. 9 [34].

Near the saturation temperature  $T_9 = 0.62$ , the  $(n, \gamma)$  reaction rate is several orders of magnitude larger than that of the  $^{36}\text{Mg}(\alpha, n)^{39}\text{Si}$  reaction. Therefore, the  $(n, \gamma)$   $\beta$ -decay reaction flow is highly unlikely to be broken at the  $^{36}\text{Mg}$  isotope and the reaction path of the  $r$ -process can go to Mg isotopes with mass numbers larger than 36 that are even closer to the corresponding neutron-drip line.

#### V. ACKNOWLEDGMENTS

This work was supported by the Science and Engineering Research Board (SERB), Department of Science and Technology, Government of India under Grant Nos. SR/S2/HEP-040/2012 and SB/S2/HEP-024/2013. One of us (Shubhchintak) is supported by the U.S. National Science Foundation (NSF) Grant No. PHY-1415656 and the U.S. Department of Energy (DOE) Grant No. DE-FG02-08ER41533. We thank Peter Mohr for several useful correspondences.

- [1] J. J. Cowan, F.-K. Thielemann, and J. W. Truran, Phys. Rep. **208**, 267 (1991).  
 [2] K. Langanke and M. Wiescher, Rep. Prog. Phys. **64**, 1657 (2001).

- [3] M. Arnould, S. Goriely, and K. Takahashi, Phys. Rep. **450**, 97 (2007).  
 [4] B. S. Meyer, G. J. Mathews, W. M. Howard, S. E. Woosely and R. D. Hofmann, Astrophys. J. **399**, 656 (1992).



- [5] S. E. Wooseley, J. R. Wilson, G. J. Mathews, R. D. Hoffman, and B. S. Meyer, *Astrophys. J.* **433**, 229 (1994).
- [6] M. Terasawa, K. Sumiyoshi, T. Kajino, G. J. Mathews, and I. Tanihata, *Astrophys. J.* **562**, 470 (2001).
- [7] T. Sasaqui, T. Kajino, G. J. Mathews, K. Otsuki and T. Nakamura, *Astrophys. J.* **634**, 1173 (2005).
- [8] S. Mosby *et al.*, *Nucl. Phys. A* **909**, 69 (2013).
- [9] T. Suzuki, T. Otsuka, C. Yuan, N. Alahari, *Phys. Lett. B* **753**, 199 (2016).
- [10] T. Baumann *et al.*, *Nature*, **449**, 1022 (2007).
- [11] P. Doornenbal *et al.*, *Phys. Rev. Lett.* **111**, 212502 (2013).
- [12] G. Baur, C. A. Bertulani and H. Rebel, *Nucl. Phys. A* **584**, (1986) 188.
- [13] G. Baur, K. Hencken and D. Trautmann, *Prog. Part. Nucl. Phys.* **51**, (2003) 487.
- [14] G. Baur and S. Typel, *J. Phys. G* **35**, (2008) 014028.
- [15] F. Schümann *et al.*, *Phys. Rev. C* **73**, 015806 (2006).
- [16] T. Nakamura *et al.*, *Phys. Rev. Lett.* **83**, 1112 (1999).
- [17] N. Kobayashi *et al.*, *Phys. Rev. Lett.* **112**, 242501 (2014).
- [18] Shubhchintak and R. Chatterjee, *Nucl. Phys. A* **922**, 99 (2014).
- [19] Shubhchintak, Neelam, R. Chatterjee, R. Shyam, and K. Tsushima, *Nucl. Phys.* **939**, 101 (2015).
- [20] T. Rauscher, *At. Data. Nucl. Data Tables* **79**, 47 (2001); *ibid.*, computer code NON-SMOKER available at the URL, <http://nucastro.org/nonsmoker.html>.
- [21] C. E. Rolfs and W. S. Rodney, *Couldrons in the Cosmos* (University of Chicago Press, Chicago 1988).
- [22] P. Banerjee, R. Chatterjee and R. Shyam, *Phys. Rev. C* **78**, 035804 (2008).
- [23] R. Chatterjee, P. Banerjee and R. Shyam, *Nucl. Phys. A* **675**, (2000) 477.
- [24] I. Hamamoto, *Phys. Rev. C* **69**, (2004) 041306(R) .
- [25] C. A. Bertulani, *J. Phys. G* **25**, (1999) 1959.
- [26] T. Motobayashi, *Nucl. Phys. A* **630**, 328 (1998).
- [27] R. Shyam and I. J. Thompson, *Phys. Rev. C* **59**, 2465 (1999).
- [28] C. A. Bertulani, *Phys. Rep.* **77**, 106901 (2014).
- [29] Neelam, Shubhchintak and R. Chatterjee, *Phys. Rev. C* **92**, 044615 (2015).
- [30] Prabir Banerjee, Gerhard Baur, Kai Hencken, Radhey Shyam, and Dirk Trautmann, *Phys. Rev. C* **65**, (2002) 064602.
- [31] I. Hamamoto, *Phys. Rev. C* **76**, 054319 (2007).
- [32] M. A. Nagarajan, S. M. Lenzi and A. Vitturi, *Eur. Phys. J. A* **24**, 63 (2005).
- [33] P. Capel, P. Danielewicz, and F. M. Nunes, *Phys. Rev. C* **82**, 054612 (2010).
- [34] J. Pereira and F. Montes, *Phys. Rev. C* **93**, 034611 (2016).